Hindawi
International Journal of Antennas and Propagation
Volume 2022, Article ID 8431611, 9 pages
https://doi.org/10.1155/2022/8431611

Research Article

Planar High-Gain Millimeter-Wave Slotted SIW Cavity Antenna Array with Low Sidelobe and Grating Lobe Levels

Wenyu Ma,[1] **Wenquan Cao**,[1] **Chuang Wang**,[1] **Shujie Shi**,[2] **and Bangning Zhang**[1]

[1]*College of Communication Engineering, Army Engineering University of PLA, Nanjing 210007, China*
[2]*College of Electronic Engineering, National University of Defense Technology, Hefei 230051, China*

Correspondence should be addressed to Wenquan Cao; cao_wenquan@163.com

Received 21 May 2022; Revised 10 July 2022; Accepted 31 July 2022; Published 30 August 2022

Academic Editor: Claudio Gennarelli

In this paper, a planar high-gain millimeter-wave (mmW) slotted substrate integrated waveguide (SIW) cavity antenna array with low sidelobe and grating lobe levels is proposed. The antenna consists of a slotted SIW resonator and an SIW transmission line (TL). To achieve a high gain and simplify the structure of the antenna element, the slotted SIW cavity is resonated in high-order mode. Then, a high-gain antenna array is implemented with only four such elements. By analyzing the pattern multiplication principle of the antenna array and accurately adjusting the element spacing, the high grating lobe level caused by the large spacing of the high-order mode resonator is considerably reduced. In addition, a one-four unequal amplitude power divider is introduced to further reduce the antenna array's sidelobe levels (SLLs). Finally, the proposed antenna array is fabricated for verification. The measured peak gain is 21.4 dBi at 27.3 GHz. The measured grating lobe level in the E-plane is reduced to −17.9 dB, and the measured SLLs are lower than −19.1 dB.

1. Introduction

The millimeter-wave (mmW) band is defined in the range of 30–300 GHz and has very abundant bandwidth resources. mmW antennas with high resolution, good directivity, and strong anti-interference ability have been widely studied in mobile communication systems [1, 2], satellite communication systems [3, 4], and automotive radar systems [5, 6].

However, due to the serious propagation attenuation of mmW in the atmosphere, designing high-gain antennas is necessary. Many means have been presented to realize high-gain antennas. The reflector antenna, such as the paraboloid antenna and the Cassegrain antenna, is an effective method to develop a high-gain antenna [7–9], but the high profile and the bulky volume usually limit their application. The Fabry–Perot cavity antenna is usually composed of a radiator and a partially reflective surface (PRS) [10–12]. However, the antenna gain is very sensitive to the height of the loaded PRS, which is difficult to manufacture accurately in the mmW band. Apart from the above three-dimensional (3D) structures, many planar antennas, such as slot antennas [13, 14], patch antennas [15–17], and magneto-electric (ME) dipole antennas [18, 19], have been adopted to realize high gain. Planar mmW antennas usually contain a certain number of elements to achieve the desired high gain. However, with the increase in frequency and the number of elements, the losses of the feed network have become a major aspect that limits the achievable gain of the antenna arrays. On the one hand, planar mmW antennas can be fed by low-loss transmission lines (TLs), such as substrate integrated waveguides (SIWs) [20, 21], ridge gap waveguides (RGWs) [22, 23], and substrate integrated coaxial lines (SICLs) [24, 25], to reduce the transmission losses of the array. On the other hand, the antenna working in higher-order mode can be used to obtain high gain due to its larger aperture size and concise feed network [26–29]. It can also be adopted as a radiation element to simplify the feed network of the antenna array to further reduce the transmission losses [30, 31].

Nevertheless, the sidelobe cannot be ignored while realizing high-gain antenna arrays. Especially for antenna arrays with large element spacing, more serious grating lobes will appear. For the above antenna operating in higher-order

mode with high gain, the large electrical size of the antenna element leads to a serious grating lobe arising in the antenna array, which limits their practical applications.

To realize a high-gain array antenna with low sidelobe and grating lobe levels for mmW applications, a planar slotted high-order mode SIW cavity antenna array with a concise feed network based on SIW TL is proposed in this paper. In contrast from other slotted high-order mode SIW cavity antennas, the proposed antenna is implemented with a 1×4 antenna array to achieve a higher gain with low sidelobe and grating lobe levels in a compact size. By analyzing the principle of the antenna array's pattern multiplication, the grating lobe level caused by the large spacing of the high-order mode radiation elements is substantially reduced by reasonably adjusting the element spacing. An unequal amplitude power divider is introduced to further optimize the sidelobe levels (SLLs). The proposed slotted SIW cavity antenna array has the merits of low loss, high aperture efficiency, and low sidelobe and grating lobe levels. In addition, high-gain performance is achieved by only four elements in this design.

2. Antenna Design

The configuration of the proposed mmW slotted SIW cavity antenna array is shown in Figure 1. It is stacked by two layers of Rogers 5880 substrates with a relative dielectric constant of 2.2 and a loss tangent of 0.0009, which are fixed by surrounding plastic screws. The antenna consists of a 1×4 slotted SIW cavity array and a four-way power divider. The slotted SIW cavity is fed by an SIW TL through the slotted coupling structure.

2.1. Antenna Element. The structure of the proposed antenna element is shown in Figure 2, including the slotted SIW cavity and the SIW TL. The slotted SIW cavity is surrounded by a row of metallized vias with a radius of r_0 and a period of p_0. Additionally, a 4×4 slot array is etched on the top surface. The length of the radiation slot l_s is approximately half the waveguide wavelength, and the radiation slot width w_s, which has little impact on the radiation performance, is set to 0.9 mm. The radiation pattern in the E-plane (xoz), including the SLL and the position of the first nulls, is reshaped by adjusting the distances between the radiation slots and axes AA' s_1 and s_2. The metal column placed in the SIW cavity is used to enhance the impedance matching.

Similar to the structure of the leaky wave antenna (LWA) based on the SIW resonator TE_{220} mode proposed in [32], this slotted SIW cavity can be regarded as a combination of a 2×2 TE_{220} mode SIW resonator. In addition, the utilization of an SIW resonator with a higher mode can considerably reduce the number of surrounding metal columns to simplify the structure and reduce the processing cost. It can also be used to simplify the feed network and reduce the transmission losses. The slotted SIW cavity is excited by etching two identical longitudinal coupling slots along the bottom surface.

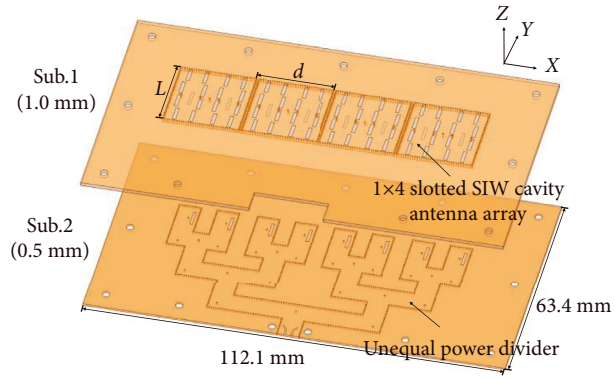

Figure 1: Configuration of the proposed antenna array.

A T-type power divider based on SIW TL is built on the bottom layer. In contrast to the microstrip TL, SIW TL can reduce the transmission losses at high frequencies and suppress the antenna's backward radiation. A two-way power divider with equal amplitude and in phase is adopted for the compactness of the feed network. The position of the coupling slots and the adjacent metal probe affect the impedance matching together. To enhance the resonance and the coupling effect, the length of the coupling slot l_c is set to approximately half of the wavelength.

The electric field distribution of the slotted SIW cavity at 26.9 GHz is shown in Figure 3. The high-order mode in SIW can be seen as two parallel TE_{20} modes with the same amplitude and phase along the BB' plane. Therefore, the proposed antenna element can be regarded as an array with two 2×4 slot antenna sub-elements. Because the sub-elements are fed by the T-type power divider in equal amplitude and phase, the spacing between the two parallel sub-elements d_s has a great influence on the SLL in the E-plane. The relationship between the distance of sub-elements d_s and the pattern in the E-plane is shown in Figure 4. The larger the spacing is, the higher the SLL is and the smaller the first null is (the closer to the boresight direction), and vice versa. The position of the first nulls of the antenna element needs to be considered when designing the low grating lobe antenna array, which is shown in Section 2.2. When taken together, the distance of sub-elements d_s is selected as $L/2$.

The simulated reflection coefficient of the antenna element is shown in Figure 5. The −10 dB impedance bandwidth is from 26.5 GHz to 27.9 GHz, and two resonant frequencies can be seen, which are generated by the resonances of the slotted SIW cavity and the slot coupling structure.

The simulated radiation patterns of the antenna element at 26.9 GHz are illustrated in Figure 6, and the simulated peak gain is achieved as 15.8 dBi. The first nulls of the E-plane are located at ±33°. The SLL in the E-plane of the antenna element is only −9.7 dB, while the SLL in the H-plane reaches −20.6 dB.

2.2. 1×4 Antenna Array with Low Sidelobe and Grating Lobe Levels. Then, an antenna array is designed to further improve the gain to meet the requirement of the mmW

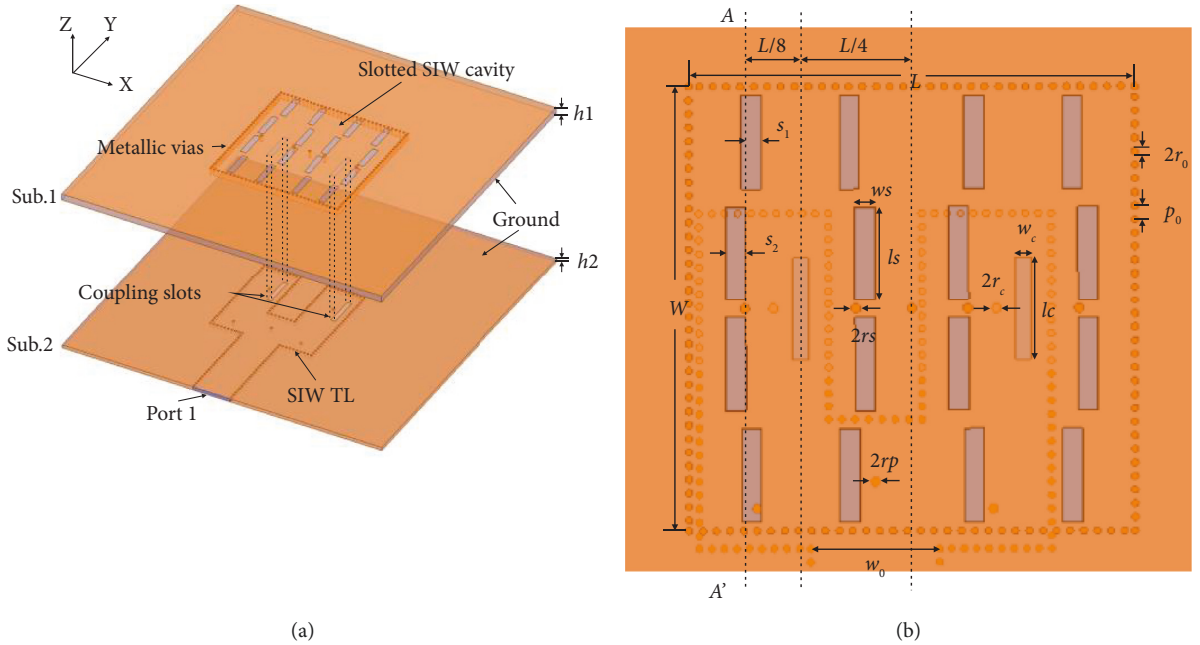

Figure 2: Configuration of the antenna element. (a) Perspective view. (b) Top view.

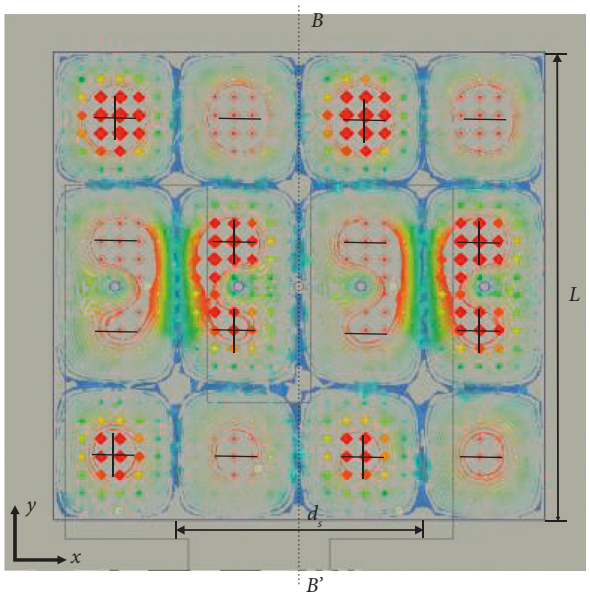

Figure 3: Simulated electric field distribution of the slotted SIW cavity at 26.9 GHz.

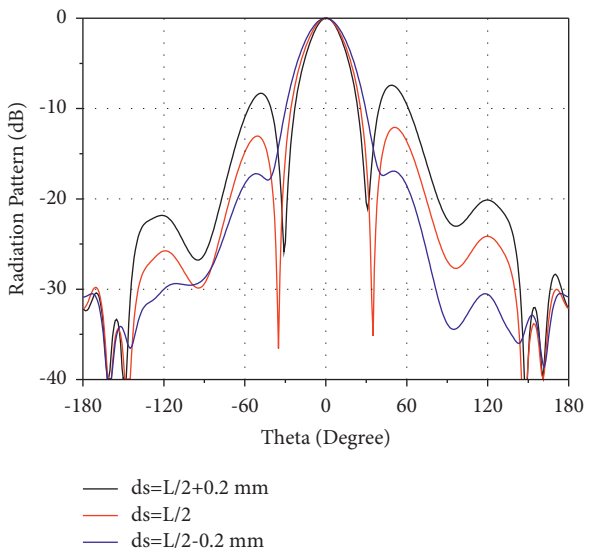

Figure 4: The relationship between the distance of sub-elements d_s and the pattern in E-plane at 26.9 GHz.

systems. According to the theory of antenna arrays, to ensure that there is no grating lobe appearing in the visible area, the spacing between the adjacent elements of a uniform antenna array cannot exceed one wavelength.

As displayed in Figure 3, the slotted SIW cavity works in a high-order mode similar to the TE_{440} mode, and the element size is approximately two wavelengths. According to the results of parameter optimization in Table 1, the aperture area of the antenna element is $1.79\lambda_0 \times 1.79\lambda_0$ (λ_0 is the wavelength in the free space at 26.9 GHz). Therefore, serious grating lobes are generated for periodic linear arrays.

However, we know that the antenna array's pattern is the multiplication of the pattern of the antenna element and the array factor. Therefore, the pattern of the antenna array is affected not only by the array factor F_a, which is determined by the spacing between the adjacent elements, but also by the result of the combined action of the element pattern and the array factor. The principle of pattern multiplication is depicted in Figure 7. Fortunately, when the grating lobe of the array factor coincides with the first null position of the element pattern, a serious grating lobe in the pattern of the antenna array is effectively suppressed.

For a uniform linear array, the expression of the normalized array factor is as follows:

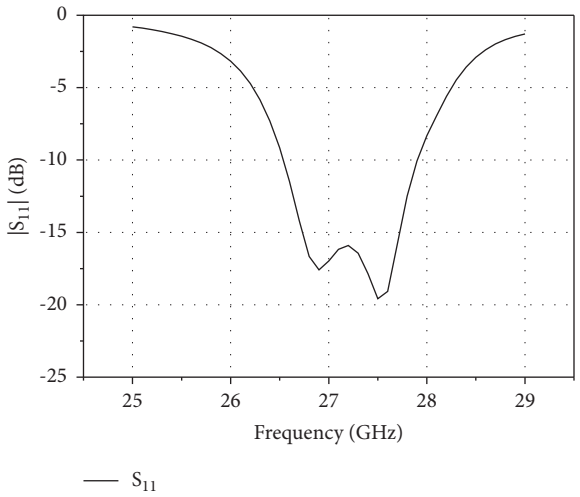

Figure 5: Simulated $|S_{11}|$ of the slotted SIW cavity.

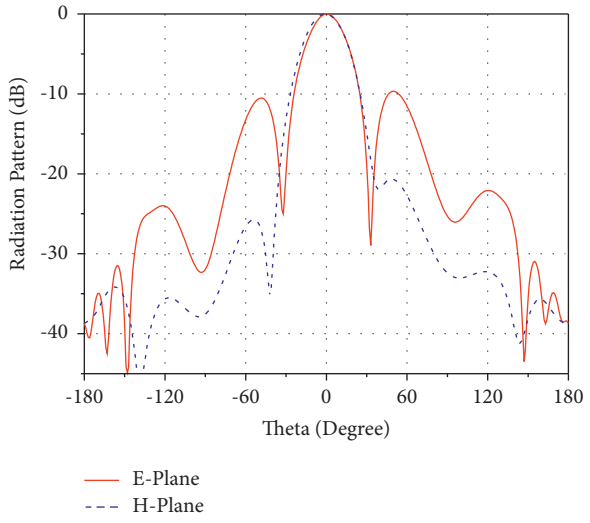

Figure 6: Radiation patterns of antenna element at 26.9 GHz.

Table 1: Parameters of the presented antenna element (unit: mm).

Parameters	L	W	w_0	r_p	l_s	w_s
Values	20	20	5.8	0.2	4.2	0.9
Parameters	s_1	s_2	r_s	l_c	w_c	r_c
Values	0.3	0.4	0.2	4.6	0.7	0.2
Parameters	d_s	p_0	r_0	d	h_1	h_2
Values	10	0.6	0.15	20.7	1	0.5

$$F_a = \frac{\sin Nu/2}{N \sin u/2}, \qquad u = kd\cos\theta + \varphi, \tag{1}$$

where φ represents the phase difference of excitation, θ represents the angle between the beam direction and the array axis, and d represents the distance between the adjacent elements.

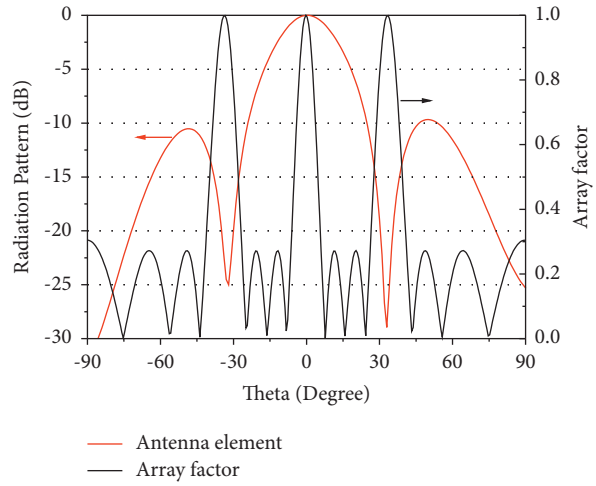

Figure 7: Principle of pattern multiplication.

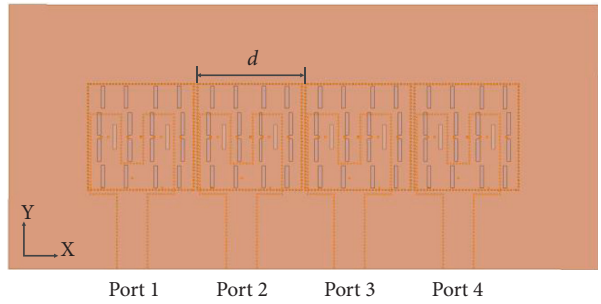

Figure 8: Structure of 1×4 antenna array.

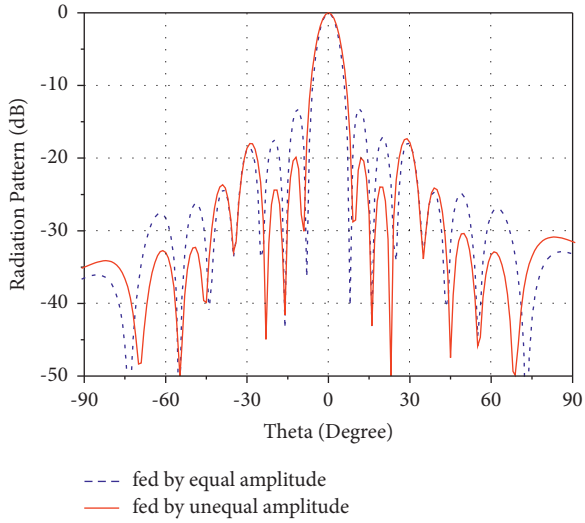

Figure 9: Radiation pattern of the antenna array fed by (a) equal amplitude (dash line) and (b) unequal amplitude (solid line).

When $u = 0$, the array factor reaches the maximum. The relationship between the distance between adjacent elements d and the direction of grating lobe θ is as follows:

$$\theta_m = \cos^{-1}\left[\frac{1}{kd}(-\varphi \pm 2m\pi)\right], \quad i = 1, 2, 3, \ldots, \tag{2}$$

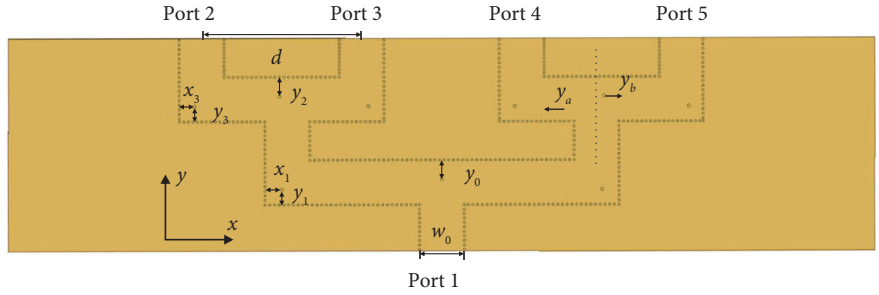

Figure 10: Configuration of the four-way unequal power divider.

Table 2: Dimensions of the unequal power divider (unit: mm).

Parameters	w_0	d	y_0	x_1	y_1
Values	5.8	20.7	2.5	2.2	2
Parameters	y_2	x_3	y_3	y_a	y_b
Values	2.5	2	2	0.7	1

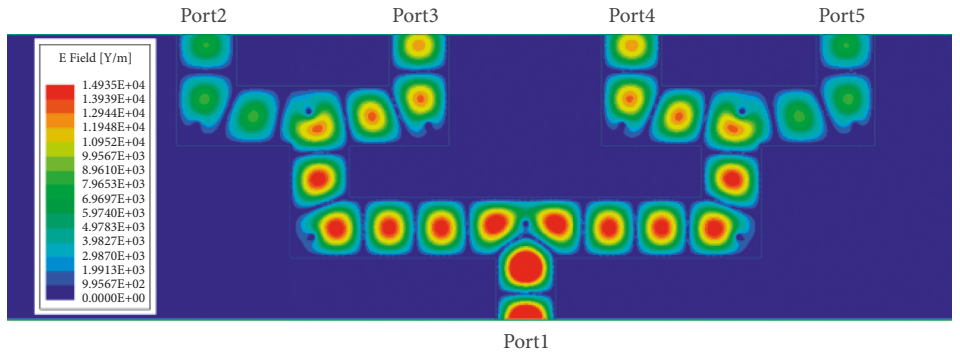

Figure 11: Magnitude E-field distribution of the unequal power divider at 27 GHz.

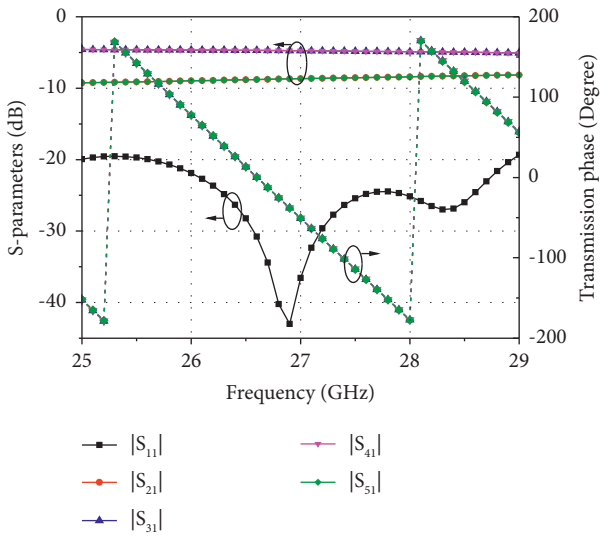

Figure 12: Simulated S-parameters of the unequal power divider.

where $i = 0$ represents the main lobe and $i = 1, 2, 3, \ldots$ refers to the grating lobe.

The transverse dimension of the antenna element designed above is $1.79\lambda_0$. Therefore, when the spacing of the adjacent element is $1.86\lambda_0$, that is, $d = 20.7$ mm, the direction of the grating lobe is as follows:

$$\theta_1 = \cos^{-1}\left[\frac{1}{2\pi/\lambda_0 \cdot 1.86\lambda_0}(\pm 2\pi)\right] = 56.25^\circ, 123.75^\circ. \quad (3)$$

The angle converted to the normal direction of the array axis is $\pm 33.75^\circ$. It is located just near the position of the first nulls in the E-plane of the antenna element. Due to the limitation of the antenna element size, the element spacing cannot be further reduced. However, increasing the element spacing results in more serious grating lobes.

Finally, the 1×4 antenna array is optimized by the commercial electromagnetic simulation software HFSS, and the structure is displayed in Figure 8. The element spacing is finally selected as $d = 20.7$ mm. The simulated radiation pattern in the E-plane of the antenna array fed by equal amplitude and in phase at 26.9 GHz is depicted in Figure 9 (dashed line). The grating lobe level reaches -18.47 dB at $\pm 29^\circ$; however, the SLL is only -13.28 dB.

To further reduce the SLL of the antenna array, the technique of unequal amplitude power feeding is considered. The radiation pattern of the antenna array fed by

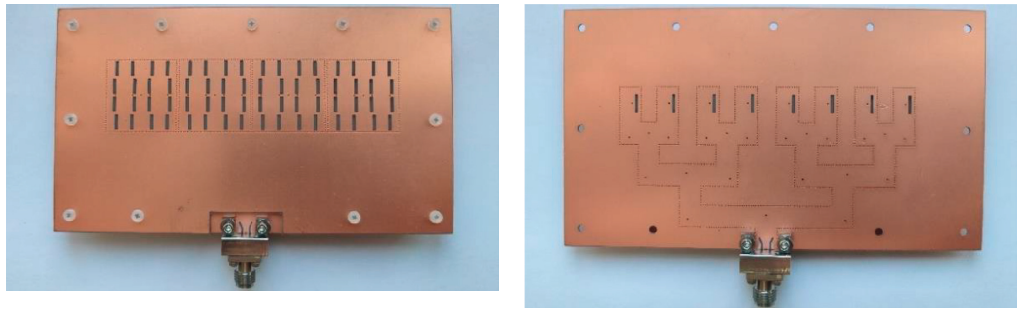

(a) (b)

Figure 13: Photograph of the proposed 1×4 antenna array. (a) Top layer. (b) Bottom layer.

unequal amplitude at 26.9 GHz is illustrated in Figure 9 (solid line), and the input power ratio of each port is set to 0.4 : 1:1 : 0.4. The power ratio is calculated according to the target SLL of −20 dB. The SLL of the array is considerably reduced to −19.9 dB, while the grating lobe level is basically unchanged at −18 dB.

3. Simulation and Experimental Results

As seen in Figure 1, a 1×4 antenna array fed by a one-four unequal power divider based on SIW TL is designed. The configuration of the one-four unequal power divider is displayed in Figure 10. The design principle of a multi-channel unequal power divider was analyzed in detail in [33], and an extra description is no longer given here. Table 2 summarizes the final dimensions of the unequal power divider.

The simulated magnitude E-field distribution at 27 GHz is demonstrated in Figure 11. The four output ports of the designed power divider have unequal amplitude and in-phase performance. From a quantitative perspective, the simulated S-parameters of the unequal power divider are plotted in Figure 12. Good impedance matching can be obtained in the range of 25–29 GHz, and the amplitude difference between the output ports is approximately 3.96 dB, which corresponds to an output power ratio of 1 : 0.4. In addition, the phase difference between the output ports is basically 0°.

The antenna array is fabricated and demonstrated in Figure 13, and a GCPW-SIW transition structure is designed for measurement. The antenna array is measured by using a 2.92 mm end-launch connector.

The simulated and measured $|S_{11}|$ and the gains of the 1×4 antenna array are depicted in Figure 14. The simulated −10−dB impedance bandwidth is from 26.6 GHz to 27.8 GHz, and the measured value ranges from 26.9 GHz to 28.1 GHz. Compared with the simulated results, the measurements move toward high frequencies, which may be caused by the fluctuation of the dielectric constant and the fabrication tolerance. Because the dielectric constant of the PCB laminate fluctuates at a high frequency, the value decreases slightly with an increasing frequency. The simulated $|S_{11}|$ and the gains of the 1×4 antenna array with different dielectric constants are shown in Figure 15. When the

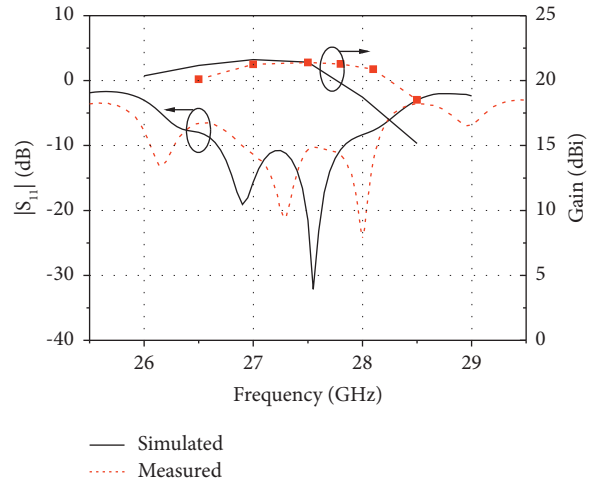

Figure 14: Simulated and measured $|S_{11}|$ and gains of the 1×4 antenna array.

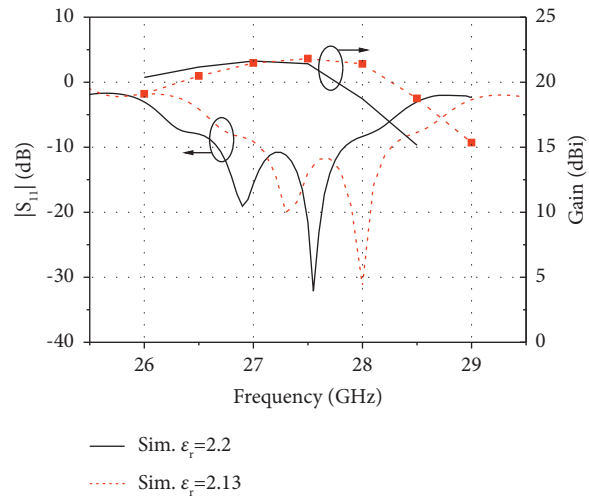

Figure 15: Simulated $|S_{11}|$ and gains of the 1×4 antenna array with different dielectric constants.

dielectric constant is set to 2.13, the simulation results move toward high frequency, which is almost consistent with the measurement results in Figure 14. The variation trends of the simulated and the measured gains are relatively consistent

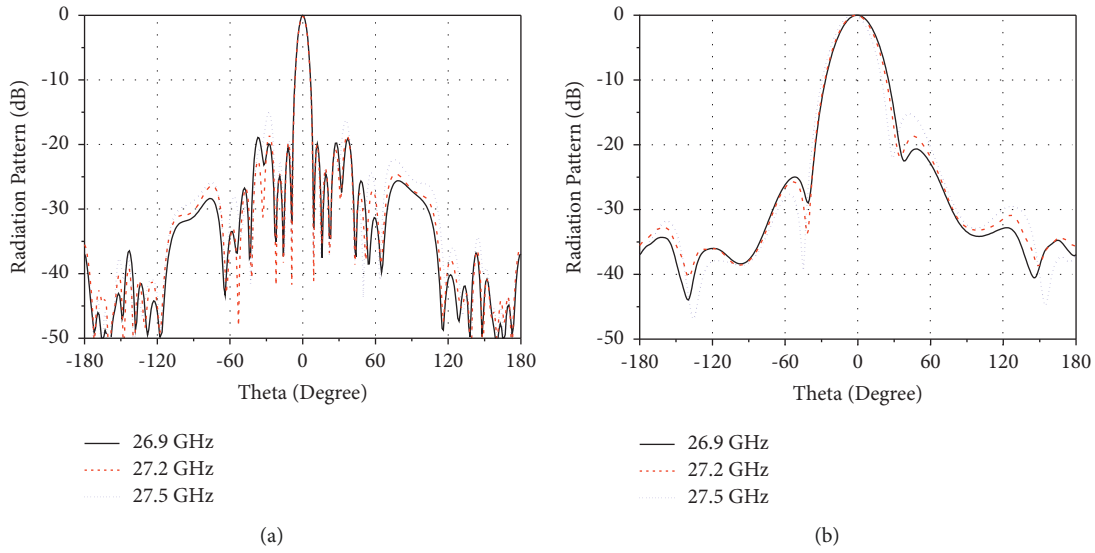

Figure 16: Simulated radiation patterns of the proposed 1×4 antenna array. (a) E-plane (*xoz*). (b) H-plane (*yoz*).

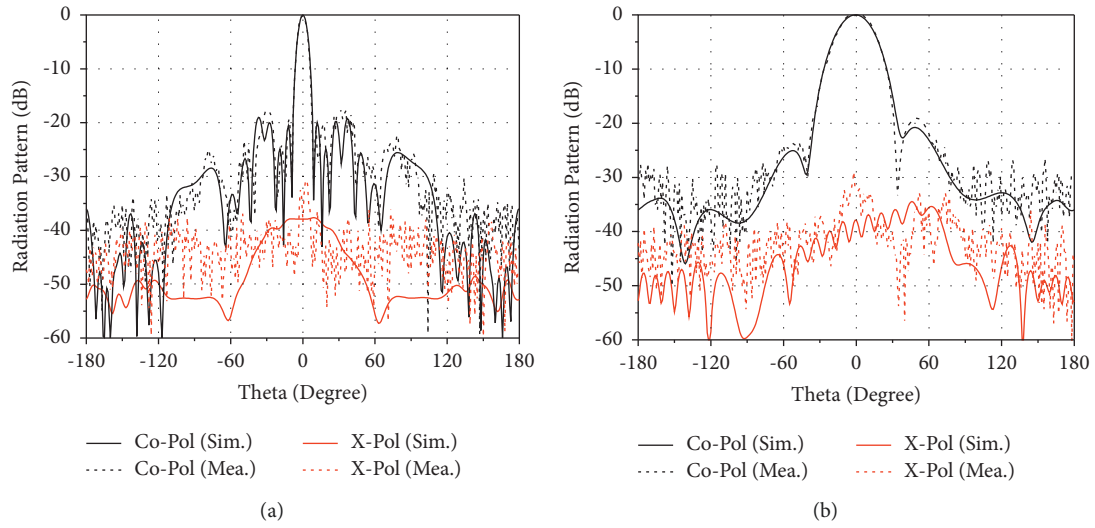

Figure 17: Simulated radiation patterns at 26.9 GHz (solid line) and measured one at 27.3 GHz (dash line) of the proposed 1×4 antenna array. (a) E-plane (*xoz*). (b) H-plane (*yoz*).

within the operating band. Errors between the two may be caused by manufacturing errors and measurement errors. The maximum gain is 21.4 dBi, and the gain is greater than 19.8 dBi in the working band. The simulated radiation efficiency is higher than 89%.

The simulated radiation patterns of the proposed 1×4 antenna array at 26.9 GHz, 27.2 GHz, and 27.5 GHz are plotted in Figure 16. As the frequency increases, the grating lobe levels and the SLLs increase, which is caused by the increase in spacing between antenna elements. However, in the whole working band, the grating lobe levels in the E-plane are still lower than −15.1 dB, and the SLLs in the E- and H-planes are lower than −19.4 dB and −15.2 dB, respectively.

As shown in Figure 17, the solid line and the dashed line represent the simulated patterns at 26.9 GHz and the measured patterns at 27.3 GHz. The measured results are in good agreement with the simulation results. The measured peak gain is 21.4 dBi at 27.3 GHz. The measured grating lobe levels in the E-plane are −17.9 dB, while the simulated level is −19 dB. The difference between them may be caused by the measurement error and the increase in the measurement frequency. The measured SLLs in the E and H-planes are −19.5 dB and −19.1 dB, respectively. In addition, the cross-polarization levels in both the E and the H-planes are all lower than approximately −30 dB.

Table 3 illustrates the comparison of our proposed antenna array with other planar mmW antenna arrays in the literature. The mmW antenna arrays proposed in [18, 22] achieve a higher gain, but with a larger number of elements and higher SLLs. Compared with other high-order mode

Table 3: Performance comparison with other reported planar MMW antenna arrays.

Ref.	Type	Freq. (GHz)	No. of elements	Peak gain (dBi)	Sidelobe/grating lobe level (dB)	Aperture Eff. (%)	Size (λ_0)
[15]	SIW (patch)	60	4×4	19.6	−13	65	3.26×3.42
[17]	Empty SIW (patch)	28.25	4×4	18.2	∼−10	32.4	4.06×4.0
[18]	SIW (ME-dipole)	60	8×8	26.1	∼−10	77.8	6.8×6.12
[22]	RGW (slot)	60	16×16	32.5	−13	70	1.6×1.65
[25]	SICL (patch)	41.5	6×6	17.6	−20.4	26.9	4.56×3.73
[30]	SIW (slot)	45	2×4	21.7	−12	76.2	4.0×3.86
[31]	SIC (spiral antenna)	60	2×2	20	∼ −10	55.6	3.87×3.7
[33]	SIW (patch)	28	1×8	13.97	−20	15.8	$\sim6.6\times1.9$
Proposed	SIW (slotted high-order mode cavity)	27.3	1×4	21.4	−17.9	78	7.6×1.85

*The aperture efficiency is calculated as $(G\times\lambda_0{}^2)/(4\pi\times A_p)$.

SIW cavity arrays presented in [30, 31], the proposed one shows lower grating lobe levels. The antenna arrays in [25, 33] have lower SLLs, but the multilayer structure and the relatively low aperture efficiency limit their applications. In comparison, our slotted SIW cavity antenna array has lower sidelobe and grating lobe levels and achieves the highest aperture efficiency among the various designs. In addition, the peak realized gain of 21.4 dBi is generated by only four antenna elements in our design, while 8 or even more than 16 antenna elements are needed for traditional antenna arrays.

4. Conclusion

In this paper, a planar high-gain slotted SIW cavity antenna array for mmW applications is proposed and designed. By using the slotted cavity based on the SIW resonator high-order mode, the gain and radiation efficiency are substantially improved, and the feed network can be simplified. By analyzing the pattern multiplication theorem of the antenna array, a low grating lobe of the array with large element spacing is realized. The SLL is further reduced by an unequal power feed. The designed antenna array has the advantages of high gain, high aperture efficiency, low loss, and low sidelobe and grating lobe levels, which are suitable for various mmW applications.

Data Availability

The data used to support the findings of this study are included within the article.

Conflicts of Interest

The authors declare that they have no conflicts of interest.

Acknowledgments

This study was supported by the National Natural Science Foundation of China (grant nos. 61871399 and 61401506) and Research Program of National University of Defense Technology (ZK20-22).

References

[1] W. Hong, Z. H. Jiang, C. Yu, J. Zhou, P. Chen, and Z. Yu, "Multibeam antenna technologies for 5G wireless communications," *IEEE Transactions on Antennas and Propagation*, vol. 65, no. 12, pp. 6231–6249, 2017.

[2] B. Yang, Z. Yu, J. Lan, R. Zhang, J. Zhou, and W. Hong, "Digital beamforming-based massive MIMO transceiver for 5G millimeter-wave communications," *IEEE Transactions on Microwave Theory and Techniques*, vol. 66, no. 7, pp. 391–403, 2018.

[3] Y. B. Jung, A. V. Shishlov, and S. O. Park, "Cassegrain antenna with hybrid beam steering scheme for mobile satellite communications," *IEEE Transactions on Antennas and Propagation*, vol. 57, no. 5, pp. 1367–1372, 2009.

[4] Y. Ding, N. B. Buchanan, V. F. Fusco, R. Baggen, M. Martinez-Vazquez, and M. van der Vorst, "Analog/Digital hybrid delay-locked-loop for K/Ka band satellite retrodirective arrays," *IEEE Transactions on Microwave Theory and Techniques*, vol. 66, no. 7, pp. 3323–3331, 2018.

[5] J. Hasch, E. Topak, R. Schnabel, T. Zwick, R. Weigel, and C. Waldschmidt, "Millimeter-wave technology for automotive radar sensors in the 77 GHz frequency band," *IEEE Transactions on Microwave Theory and Techniques*, vol. 60, no. 3, pp. 845–860, 2012.

[6] J. Xu, W. Hong, H. Zhang, G. Wang, Y. Yu, and Z. H. Jiang, "An array antenna for both long- and medium-range 77 GHz automotive radar applications," *IEEE Transactions on Antennas and Propagation*, vol. 65, no. 12, pp. 7207–7216, 2017.

[7] Y. Bi, Y. Li, and J. Wang, "3-D printed wideband Cassegrain antenna with a concave subreflector for 5G millimeter-wave 2-D multibeam applications," *IEEE Transactions on Antennas and Propagation*, vol. 68, no. 6, pp. 4362–4371, 2020.

[8] P. Zheng, G. Q. Zhao, S. H. Xu, F. Yang, and H. J. Sun, "Design of a W-band full-polarization monopulse Cassegrain antenna," *IEEE Antennas and Wireless Propagation Letters*, vol. 16, pp. 99–103, 2017.

[9] T. P. Nguyen, C. Pichot, C. Migliaccio, and W. Menzel, "Study of folded reflector multibeam antenna with dielectric rods as primary source," *IEEE Antennas and Wireless Propagation Letters*, vol. 8, pp. 786–789, 2009.

[10] Y. Lee, X. Lu, Y. Hao, S. Yang, J. R. G. Evans, and C. G. Parini, "Low-profile directive millimeter-wave antennas using free-formed three-dimensional (3-D) electromagnetic bandgap structures," *IEEE Transactions on Antennas and Propagation*, vol. 57, no. 10, pp. 2893–2903, 2009.

[11] A. Hosseini, F. Capolino, and F. De Flaviis, "Gain enhancement of a V-band Antenna using a fabry-pérot cavity with a self-sustained all-metal cap with FSS," *IEEE Transactions on Antennas and Propagation*, vol. 63, no. 3, pp. 909–921, 2015.

[12] A. Goudarzi, M. M. Honari, and R. Mirzavand, "A millimeter-wave fabry–perot cavity antenna with unidirectional beam scanning capability for 5G applications," *IEEE Transactions on Antennas and Propagation*, vol. 70, no. 3, pp. 1787–1796, 2022.

[13] Y. J. Cheng, W. Hong, and K. Wu, "94 GHz substrate integrated monopulse antenna array," *IEEE Transactions on Antennas and Propagation*, vol. 60, no. 1, pp. 121–129, 2012.

[14] Z. J. Guo and Z. C. Hao, "A compact wideband millimeter-wave substrate-integrated double-line slot array antenna," *IEEE Transactions on Antennas and Propagation*, vol. 69, no. 2, pp. 882–891, 2021.

[15] Y. Li and K. M. Luk, "Low-Cost high-gain and broadband substrate- integrated-waveguide-fed patch antenna array for 60-GHz band," *IEEE Transactions on Antennas and Propagation*, vol. 62, no. 11, pp. 5531–5538, 2014.

[16] A. Chen, Y. Zhang, Z. Chen, and C. Yang, "Development of a *ka*-band wideband circularly polarized 64-element microstrip antenna array with double application of the sequential rotation feeding technique," *IEEE Antennas and Wireless Propagation Letters*, vol. 10, pp. 1270–1273, 2011.

[17] Z. U. Khan, T. H. Loh, A. Belenguer, and A. Alomainy, "Empty substrate-integrated waveguide-fed patch antenna array for 5G millimeter-wave communication systems," *IEEE Antennas and Wireless Propagation Letters*, vol. 19, no. 5, pp. 776–780, 2020.

[18] Y. Li and K. M. Luk, "A 60-GHz wideband circularly polarized aperture-coupled magneto-electric dipole antenna array," *IEEE Transactions on Antennas and Propagation*, vol. 64, no. 4, pp. 1325–1333, 2016.

[19] Q. Zhu, K. B. Ng, C. H. Chan, and K. M. Luk, "Substrate-integrated-waveguide-fed array antenna covering 57–71 GHz band for 5G applications," *IEEE Transactions on Antennas and Propagation*, vol. 65, no. 12, pp. 6298–6306, 2017.

[20] D. Deslandes and K. Wu, "Integrated microstrip and rectangular waveguide in planar form," *IEEE Microwave and Wireless Components Letters*, vol. 11, no. 2, pp. 68–70, 2001.

[21] F. Xu and K. Wu, "Guided-wave and leakage characteristics of substrate integrated waveguide," *IEEE Transactions on Microwave Theory and Techniques*, vol. 53, no. 1, pp. 66–73, 2005.

[22] D. Zarifi, A. Farahbakhsh, A. U. Zaman, and P. S. Kildal, "Design and fabrication of a high-gain 60-GHz corrugated slot antenna array with ridge gap waveguide distribution layer," *IEEE Transactions on Antennas and Propagation*, vol. 64, no. 7, pp. 2905–2913, 2016.

[23] M. M. M. Ali and A. Sebak, "Printed RGW circularly polarized differential feeding antenna array for 5G communications," *IEEE Transactions on Antennas and Propagation*, vol. 67, no. 5, pp. 3151–3160, 2019.

[24] T. Zhang, Y. Zhang, W. Hong, and K. Wu, "Wideband millimeter-wave SIW cavity backed patch antenna fed by substrate integrated coaxial line," in *Proceedings of the IEEE International Wireless Symposium (IWS 2015)*, pp. 1–4, Shenzhen, China, March 2015.

[25] K. Xing, B. Liu, Z. Guo, X. Wei, R. Zhao, and Y. Ma, "Backlobe and sidelobe suppression of a Q-band patch antenna array by using substrate integrated coaxial line feeding technique," *IEEE Antennas and Wireless Propagation Letters*, vol. 16, pp. 3043–3046, 2017.

[26] X. Zhang, L. Zhu, and Q. S. Wu, "Sidelobe-reduced and gain-enhanced square patch antennas with adjustable beamwidth under TM03 mode operation," *IEEE Transactions on Antennas and Propagation*, vol. 66, no. 4, pp. 1704–1713, 2018.

[27] W. Han, F. Yang, J. Ouyang, and P. Yang, "Low-cost wideband and high-gain slotted cavity antenna using high-order modes for millimeter-wave application," *IEEE Transactions on Antennas and Propagation*, vol. 63, no. 11, pp. 4624–4631, 2015.

[28] M. Asaadi and A. Sebak, "High-gain low-profile circularly polarized slotted SIW cavity antenna for MMW applications," *IEEE Antennas and Wireless Propagation Letters*, vol. 16, pp. 752–755, 2017.

[29] P. Wu, S. Liao, and Q. Xue, "Wideband excitations of higher-order mode substrate integrated waveguides and their applications to antenna array design," *IEEE Transactions on Antennas and Propagation*, vol. 65, no. 8, pp. 4038–4047, 2017.

[30] Q. Li, C. Liu, Y. Luo, Y. Zhang, and W. Hong, "Substrate integrated cavity backed slot antenna with high-order mode for Q-band 5G communications," in *Proceedings of the 9th Asia-Pacific Conference on Antennas and Propagation (APCAP)*, pp. 1-2, Xiamen, China, August 2020.

[31] J. Zhu, S. Liao, S. Li, and Q. Xue, "60 GHz wideband high-gain circularly polarized antenna array with substrate integrated cavity excitation," *IEEE Antennas and Wireless Propagation Letters*, vol. 17, no. 5, pp. 751–755, 2018.

[32] W. Ma, W. Cao, S. Shi, and X. Yang, "Compact high gain leaky-wave antennas based on substrate integrated waveguide TE_{220} mode," *IEEE Access*, vol. 7, Article ID 145060, 2019.

[33] S. J. Park, D. H. Shin, and S. O. Park, "Low side-lobe substrate-integrated-waveguide antenna array using broadband unequal feeding network for millimeter-wave handset device," *IEEE Transactions on Antennas and Propagation*, vol. 64, no. 3, pp. 923–932, 2016.